CALIBRATION AND EQUALISATION OF PLASTIC SCINTILLATOR DETECTORS FOR ANTIPROTON ANNIHILATION IDENTIFICATION OVER POSITRON/POSITRONIUM BACKGROUND*

Nicola Zurlo[a,b,†], C. Amsler[c], M. Antonello[d,e], A. Belov[f], G. Bonomi[b,g] R.S. Brusa[h,i], M. Caccia[d,e], A. Camper[j], R. Caravita[j], F. Castelli[d,k] G. Cerchiari[l], D. Comparat[m], G. Consolati[d,n], A. Demetrio[o], L. Di Noto[p,q] M. Doser[j], M. Fanì[j,p,q], R. Ferragut[d,r], S. Gerber[j], M. Giammarchi[d] A. Gligorova[c], L. Gloggler[j], F. Guatieri[h,i], S. Haider[j], A. Hinterberger[j] A. Kellerbauer[l], O. Khalidova[j], D. Krasnický[p], V. Lagomarsino[p,q] C. Malbrunot[j], S. Mariazzi[h,i], V. Matveev[f,s], S.R. Müller[l], G. Nebbia[t] P. Nedelec[u], M. Oberthaler[o], E. Oswald[j], D. Pagano[b,g], L. Penasa[h,i] V. Petracek[v], F. Prelz[d], M. Prevedelli[w], B. Rienaecker[j] , O.M. Røhne[x] A. Rotondi[b,y], H. Sandaker[x], R. Santoro[d,e], G. Testera[p], I.C. Tietje[j] V. Toso[d,r], T. Wolz[j], P. Yzombard[l], C. Zimmer[j]

[a]Department of Civil, Environmental, Architectural Engineering and Mathematics University of Brescia, via Branze 43, 25123 Brescia, Italy
[b]INFN Pavia, via Bassi 6, 27100 Pavia, Italy
[c]Stefan Meyer Institute for Subatomic Physics, Austrian Academy of Sciences Boltzmanngasse 3, 1090 Vienna, Austria
[d]INFN Milano, via Celoria 16, 20133 Milano, Italy
[e]Department of Science, University of Insubria, Via Valleggio 11, 22100 Como, Italy
[f]Institute for Nuclear Research of the Russian Academy of Science, Moscow 117312, Russia
[g]Department of Mechanical and Industrial Engineering, University of Brescia via Branze 38, 25123 Brescia, Italy
[h]Department of Physics, University of Trento, via Sommarive 14, 38123 Povo, Trento, Italy
[i]TIFPA/INFN Trento, via Sommarive 14, 38123 Povo, Trento, Italy
[j]Physics Department, CERN, 1211 Geneva 23, Switzerland
[k]Department of Physics "Aldo Pontremoli", University of Milano via Celoria 16, 20133 Milano, Italy
[l]Max Planck Institute for Nuclear Physics, Saupfercheckweg 1, 69117 Heidelberg, Germany
[m]Laboratoire Aimé Cotton, Université Paris-Sud, ENS Paris Saclay, CNRS Université Paris-Saclay, 91405 Orsay Cedex, France
[n]Department of Aerospace Science and Technology, Politecnico di Milano via La Masa 34, 20156 Milano, Italy
[o]Kirchhoff Institute for Physics, Heidelberg University Im Neuenheimer Feld 227, 69120 Heidelberg, Germany
[p]INFN Genova, via Dodecaneso 33, 16146 Genova, Italy
[q]Department of Physics, University of Genova, via Dodecaneso 33, 16146 Genova, Italy
[r]LNESS, Department of Physics, Politecnico di Milano, via Anzani 42, 22100 Como, Italy
[s]Joint Institute for Nuclear Research, Dubna 141980, Russia
[t]INFN Padova, via Marzolo 8, 35131 Padova, Italy
[u]Institute of Nuclear Physics, CNRS/IN2p3, University of Lyon 1, 69622 Villeurbanne, France
[v]Czech Technical University, Prague, Brehová 7, 11519 Prague 1, Czech Republic
[w]University of Bologna, Viale Berti Pichat 6/2, 40126 Bologna, Italy
[x]Department of Physics, University of Oslo, Sem Sælandsvei 24, 0371 Oslo, Norway
[y]Department of Physics, University of Pavia, via Bassi 6, 27100 Pavia, Italy

(Received October 31, 2019)

* Presented at the 3rd Jagiellonian Symposium on Fundamental and Applied Subatomic Physics, Kraków, Poland, June 23–28, 2019.

† Corresponding author: zurlo@cern.ch

In this contribution, the system of the external plastic scintillator slabs of the AEgIS experiment is presented. These slabs, surrounding the superconducting magnet and operating at room temperature, are read out by photomultiplier tubes (PMTs) that are calibrated and equalised to be exploited as a whole detector with useful segmentation and redundancy to effectively detect single antiparticle annihilations. In particular, thanks to periodically recurring calibrations with cosmic rays and to a detailed study of the system in different operational conditions, including extensive Monte Carlo (MC) simulations, these scintillators can be used to identify antiproton annihilations over the constant background represented by cosmic rays and over the strongly time-dependent background due to positrons/positronium annihilations. By means of the sampling and digitization of the analog signal produced by each phototube and the consequent analysis of the amplitude of the recorded events, the energy released by the particle in the scintillator slab can be estimated consistently and with good accuracy. As a consequence, we are able to identify an amplitude range where positrons/positronium annihilations can be univocally excluded. This prerequisite allows us to exploit the array of external plastic scintillators for antihydrogen annihilations tagging.

DOI:10.5506/APhysPolB.51.213

1. Introduction

The AEgIS Collaboration aims at producing antihydrogen ($\bar{H}$) and eventually measuring the effects of Earth's gravitational field on it. The experiment is located in the CERN Antiproton Decelerator (AD), which at the moment is the only facility providing low-energy antiproton beam in the world.

In contrast to almost all the antihydrogen experiments performed or in progress at the AD [1–6] (but with one significant exception [7]), the AEgIS experiment seeks to exploit the charge exchange reaction between an antiproton ($\bar{p}$) and a highly-excited positronium atom [8–13]

$$\bar{p} + \mathrm{Ps}^* \rightarrow \bar{H}^* + e^- \,.$$

However, differently from [7] where Ps* was produced by combining trapped positrons and cesium atoms, in AEgIS positronium[1] (Ps) is produced by implantation of a bunch of positrons (e^+) on an e^+/Ps converter (namely, a mesoporous silica target) and it is subsequently excited to a Rydberg state (Ps*) via a double step laser excitation. In the meanwhile, antiprotons are kept in a multi-ring Penning–Malmberg trap located near the e^+/Ps converter: the Ps* traverse through the perforated parts of the trap electrodes facing the converter, reaching the antiproton plasma.

[1] All along this report, with this word we refer to orthopositronium.

The main steps achieved by AEgIS towards this goal include the production of $e^+ \rightarrow$ Ps converters (in reflection [14] and in transmission [15]), a proof-of-principle experiment with antiprotons demonstrating that the deflection of antiparticles by a few μm due to an external force can be detected [16], the Ps efficient excitation to the $n = 3$ energy level [17], the compression of the antiproton plasma to high densities to maximise the $\mathrm{Ps}^*/\bar{p}$ overlap [18], and the imaging of the Ps^* velocity distribution [19].

Moreover, the theoretical framework concerning the Ps laser excitation efficiency [20] and the charge exchange probability [21, 22] have been studied in detail inside the AEgIS Collaboration itself. Recent Monte Carlo simulations [23] have shown that the expected $\bar{H}$ production yield is small (less than one per cycle) but still measurable over the background making use of the stringent time constraint due to the delayed coincidence with the e^+ injection and the laser shot (so the importance to exclude spurious signals due to the former).

2. AEgIS apparatus

The AEgIS apparatus is composed of two aligned superconducting solenoids (the first producing a 4.5 T field and the second a 1 T field), situated inside liquid helium and liquid nitrogen vessels. A sequence of multi-ring Penning–Malmberg traps is located in the bore of the solenoids (see Fig. 1): in particular the section named "$\bar{H}$ production trap" is sit-

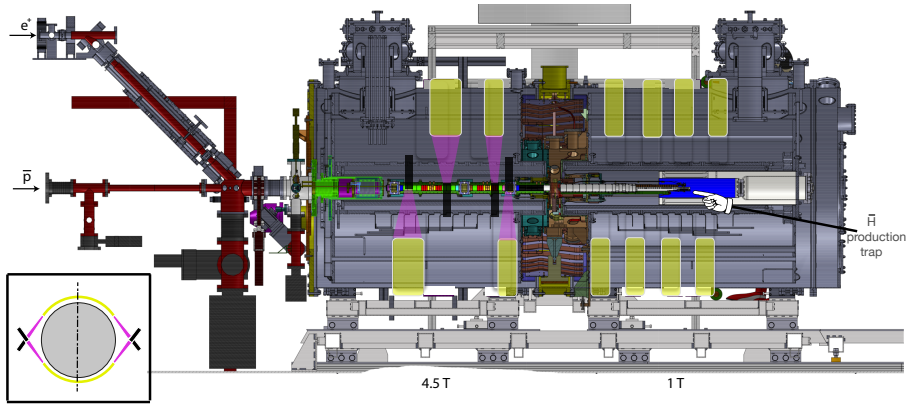

Fig. 1. (Colour on-line) Lateral view of the AEgIS apparatus. The external scintillator slabs are shown in light grey/yellow. The light guides (dark grey/purple) and the phototubes (black) are shown only for the first 4 slabs for the sake of clarity. In the small inset at the left-bottom corner, a sketch of the front view is presented (the same colour coding).

uated in the 1 T solenoid. For a full description of the AEgIS apparatus and of the complex procedures needed to make $\bar{p}$ and Ps* interact, we refer to the extensive description given in [24–26]. In the following section, we will focus on the performance of the external scintillating detector array in detecting positron, positronium and antiproton annihilation signals on top of the cosmic ray and natural radioactivity background.

3. AEgIS external scintillating detector array

The AEgIS external scintillating detector array consists of 12 arc-shaped slabs, made by EJ-200 (Eljen Technology) general-purpose, fast plastic scintillator, each of them being 1 cm thick, 10 or 20 cm wide, $\sim$ 150 cm in length. They are placed as close as possible to the apparatus (*i.e.* in contact with the external surface of the cooling vessel, at a distance of about 70 cm from the trap axis) to maximise the overall solid angle, that is $\sim$ 20% of 4π for annihilations inside the "$\bar{H}$ production trap". The slabs were read out from either side by two independent, fast and high-gain photomultipliers[2] in order to avoid spurious signals and to have good efficiency despite the light attenuation in the slabs. Each PMT has a triple magnetic field shielding and was carefully positioned and tested in order to work properly in the external magnetic field.

Since in our experiment it is essential to disentangle signals due to antiproton annihilations from positron/positronium annihilations, a deeper analysis of the signals is needed, in particular for what concerns the amplitude[3]. In fact, antiproton annihilations produce three charged particles on average, essentially minimum ionising particles going through the slab, while positron/positronium annihilations produce gamma rays that in turn produce Compton electrons in the material or inside the scintillator, thus releasing much less energy in it. Moreover, except for electrons below 100 keV and for other particles and energies irrelevant in our context, there is a direct proportionality between the energy released by the charged particle in the scintillator, the scintillator light yield and eventually the PMT signal (unless it is close to saturation, which normally was not our case) [27]. As a consequence, a threshold on the signal amplitude discriminating the two kind of annihilations can be envisaged.

[2] The PMTs were mostly XP2020 phototubes, but we installed also some Thorn-EMI 9954B, that have slightly different features, but it can be neglected for our purposes.

[3] Amplitude is intended here as the peak height of the voltage pulse produced by the PMT or, alternatively, the area below the same voltage pulse integrated in a convenient time window, in our case $\sim$ 70 ns long, measured via the integrated charge. We verified that both definitions produce results that are strongly correlated and in excellent agreement, see also footnote 5.

However, in our case the strong light attenuation inside each slab[4] caused a large uncertainty of the amplitude of the signal produced by each PMT, which made it impractical (or very detrimental in terms of efficiency) to apply any kind of method based on a threshold for single PMTs. So the following method was applied instead:

1. We calibrated the PMTs so that for each pair of them the PMT signal gain (including the light guide efficiency) was approximately the same. For the sake of simplicity, we calibrated all the PMTs to have a nearly equal gain — as defined before — and this was done with cosmic rays, see Section 4.

2. As the best proxy for the energy released in the scintillator, the average of the signal amplitude collected by the 2 PMTs reading the same slab was used. This will compensate the light attenuation effect to the first order so that we expect that the largest deviation of the average from the unattenuated value is of the order of 10% for the whole slab length. This systematical uncertainty is negligible compared to the statistical uncertainty due to the PMT avalanche process itself, and the overall signal uncertainty benefits from the averaging over two different PMTs.

3. The method described in 1. and 2. was tested with signals produced by antiprotons annihilations only and e^+/Ps annihilations only (see Sections 6 and 5, respectively); it is self-evident that a threshold to remove e^+/Ps annihilations should be as low as possible, to avoid antiproton detection efficiency losses.

4. For the most critical time window lasting about 1 ms (just after Ps* production, *i.e.* when $\bar{H}$ formation is possible), we recorded the full analog signal produced by each PMT, as a function of time, through a 12-bit-resolution 250-MHz-sampling-rate CAEN V1720 Flash ADC Waveform Digitizer [28].

5. An offline analysis was performed in order to identify (through the mentioned average method) events that have too high amplitude to be produced by e^+/Ps annihilation. They are either due to antiprotons annihilations or related to the cosmic ray background. Since the latter is known and measured very well, we can infer the number of antiproton annihilations on average. Since the $\bar{H}$ signal is temporally very well localised, this method may be applied to $\bar{H}$ too.

[4] We measured an attenuation length of 120 ± 10 cm inside each slab, that implies a factor of ~ 3 for the whole slab length.

4. Cosmic ray background signal. Calibration and equalisation

The first step was to acquire cosmic rays data. To reduce the dead time, we used a CAEN V792 Charge-to-Digital Converter (QDC, see [29]), integrating the PMT current over a ~ 70 ns window, triggered by the coincidence between two PMTs. In particular, to reduce the noise/background contribution and to be more selective on the real cosmic rays, we introduced coincidence counts between 2 PMTs reading adjacent slabs (one above the apparatus and one below, hereafter called AB setup). The corresponding spectrum is shown in Fig. 2 (a). The same configuration was simulated through the CERN MC tool Geant4 [30, 31] showing that the distribution of the energy deposited inside the scintillator was close to a Landau distribution with a maximum around 2.1 MeV, as it can be seen in the spectrum reported in Fig. 2 (b). At this stage, all PMTs supply voltages were tuned in order to have the cosmic ray peak close to 400 QDC counts (40 pC). The PMT gain drifted over time but was controlled by means of periodic calibration sessions and kept below 10%.

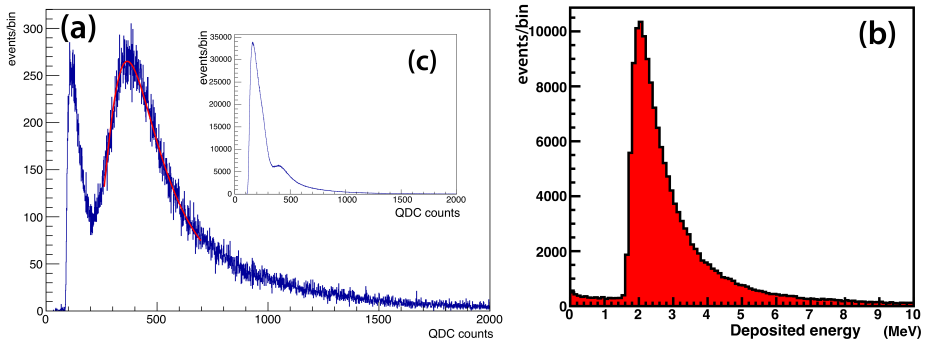

Fig. 2. Cosmic ray annihilation spectrum (distribution of the charge collected by the QDC in a 70 ns window). (a) experimental results for the AB setup (see the text for details), (b) MC simulation, (c) distribution of the average of the 2 QDC values resulting from the DOC setup (see the text for details).

The experimental spectrum corresponding to setup AB (Fig. 2 (a)) exhibits a second peak at low QDC counts, due to either a few background events or some non-ideal behaviour not included in the simulation. It is interesting to notice that the spectra taken with the QDC in the default operational configuration, *i.e.* with the coincidence of 2 PMTs reading the same slab (hereafter called DOC setup) and taking the average of the 2 PMT values after the mentioned calibration, clearly show the peak due to the cosmic rays, together with a large contribution at lower energies presumably due to natural radioactivity in the experimental area (see Fig. 2 (c), reported

in the inset). In fact, from this distribution, we can infer that $\sim 70\%$ of the events recorded are not due to real cosmic rays but to the natural radioactivity background (*e.g.* ^{40}K, now under further investigation); this may also explain why the rate of events recorded by a typical 10-cm-wide slab is ~ 65 Hz, while we expected a flux of cosmic rays of ~ 20 Hz.

5. Signal produced by positrons and positronium

In order to understand the response of the PMTs to e^+/ Ps annihilations, we acquired data just letting the positrons impinge on the e^+/ Ps converter. During this experiment, there were no antiprotons present in the "$\bar{H}$ production trap". Moreover, we had to eschew the first hundreds of ns just after the positron bunch impact on the converter, since the signal recorded by most of the PMTs reached abruptly a peak value of a few volts and remained above our threshold (50 mV) for ~ 200 ns, giving rise to PMT afterpulses. In fact, the presence of afterpulses made any measurement difficult and unreliable in the first μs.

In the time window between 1 μs and 6 μs after the positron injection, the PMTs still recorded some strong activity (~ 1 event per slab per μs on average) due to positrons reflected by the converter, bouncing again at the interface between the two solenoids by magnetic mirror effect, and impacting again on the converter, with possible positronium formation. The analysis of the pulses in the data collected by the digitizer was done within the usual DOC setup. In Fig. 3 (a), we show the spectrum obtained by the average of the peak height measured by the 2 PMTs, summed up over all the slabs[5].

Recording large statistics ($\sim 10^5$ e^+/ Ps annihilation signals), including a conservative estimation of the number of cosmic rays passing through the slabs during the measurement[6] and of the number of two simultaneous (< 10 ns) signals in the same slab, we established that e^+/ Ps signal under no circumstance exceeds 250 mV. This is in fair agreement with the Geant4 MC simulations of positron annihilation on the converter, depicted in Fig. 3 (b). Simulations with Ps were not performed, but we know that the energy carried by each gamma ray is certainly smaller, as well as the signal produced in the slab, so our procedure is certainly conservative in this respect.

[5] Differently from the spectra in Fig. 2 (a) and Fig. 2 (c), the spectra plotted in Fig. 3 (a) and Fig. 4 (a) are derived from the peak height instead of the peak area. A number of measurements were performed to establish and cross-check the connection between the two (a signal with 1 mV peak height produces around 0.2 pC of integrated charge; since the measurement with the QDC needs the addition of one extra splitter that halves the charge collected by the QDC, 1 mV in figures 3 (a) and 4 (a) corresponds to 0.1 pC = 1 QDC count in Figs. 2 (a) and 2 (c)).

[6] In the mentioned temporal window, we expect ~ 1 cosmic ray in every 10^4 gamma ray signals.

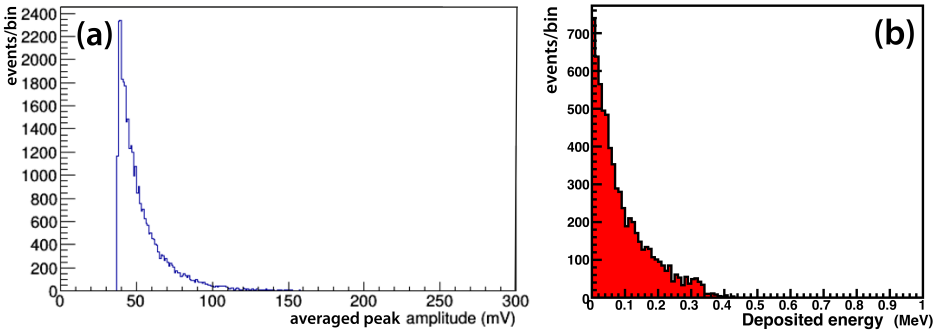

Fig. 3. e^+/Ps annihilation spectrum (distribution of the average peak height, simultaneously recorded by the 2 PMTs in the DOC setup). (a) experimental results, (b) Monte Carlo simulation in the case of only e^+.

6. Signal produced by antiprotons

Data were taken with the aim of determining the response of the PMTs to antiproton annihilations by deliberately making antiprotons annihilate on the Penning trap walls (each antiproton annihilation produces ~ 3 charged pions and ~ 2 neutral pions on average, see *e.g.* [32]). The controlled losses were induced on the trapped antiproton plasma in order to generate annihilations with a rate much higher than the one associated with the cosmic rays. At the same time, we avoided a too high annihilation rate, since this would produce simultaneous annihilations of more than one antiproton on a 10 ns time scale, or would induce PMT discharge effects. In a typical run dedicated to this measurement, all the ($\sim 10^5$) antiprotons annihilated in a fraction of a second, giving rise to an annihiliation rate of some hundreds of kHz, corresponding to a rate of some tens of kHz per slab. Higher annihilation rates were avoided because we observed the onset of PMT discharge effects and consequent non-linearity. Since the digitiser acquisition time was limited to ~ 5 ms (1310720 samples), we acquired around one hundred antiproton annihilation events per slab and per trial.

This measurement was performed with the digitizer (like for positrons), but a trial with the QDC (like for cosmic rays) gave comparable results. In Fig. 4 (a), we show the distribution of the average of the peak height amplitudes of the signals recorded in coincidence by the 2 PMTs in the standard DOC setup. Moreover, we checked that the distribution obtained averaging the signal of each couple of PMTs was compatible with the overall distribution, confirming the effectiveness of our calibration–equalization procedure.

Besides, for this scenario, a detailed MC simulation of the $\bar{p}$ annihilations was performed by means of a code based on Geant4 (Fig. 4 (b)). The experimental and the simulated distributions are in very good agreement, both

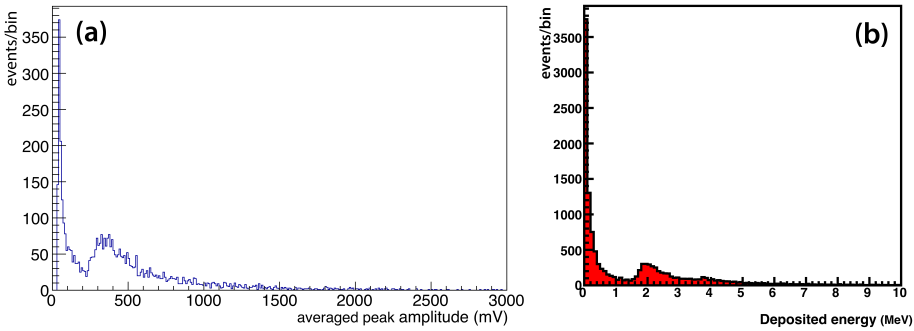

Fig. 4. Antiproton annihilation spectrum (with the standard DOC setup; see caption of Fig. 3). (a) experimental results, (b) MC simulation.

showing a low amplitude component (probably due to low-energy particles) and a high amplitude component (due to minimum ionizing particles) with a clear minimum separating the two peaks.

We emphasize that the high amplitude component is quite similar to the distribution measured/simulated for cosmic rays presented in Fig. 2 (*cf.* footnote 5 for the unit conversion); in fact, they both originate from MIPs (namely pions here and muons for cosmic rays).

7. Conclusions

The response of the AEgIS array of external plastic scintillators, each of them being coupled to two PMTs through two convenient light guides, has been investigated in different experimental conditions. First, the standard detector background has been explored and two main components have been identified: cosmic rays and natural radioactivity in the surrounding supervised area, under investigation now to pinpoint the real source. Then, we have made experiments in the presence of positrons/positronium annihilations and, finally, in the presence of antiprotons annihilations.

We have shown that recording the signal produced by all the PMTs and making the average of the signals produced by 2 PMTs reading the same slab to compensate for the light attenuation inside each slab, we were able to establish a threshold that allows us to reject *all* the events due to e^+/Ps annihilation. Depending on the performed measurement, this threshold may be defined equivalently by the peak height or by the pulse area, *i.e.* the overall charge. Using this threshold (typically, 250 mV or 25 pC for unsplit signals, after a reliable equalisation of all the PMTs) will select for signals generated by cosmic rays or antiprotons annihilations, with efficiency losses that, for antiprotons, are around 30% with respect to the highest efficiency achievable with the lowest possible threshold (50 mV).

This paves the way for making use of the array of external plastic scintillators for the detection of antihydrogen, starting from 1 μs after the positron bunch injection onwards, rigorously allowing us to avoid the strong background of signals produced by reflected positrons and positronium.

REFERENCES

[1] M. Amoretti *et al.*, *Nature* **419**, 456 (2002).

[2] G. Gabrielse *et al.*, *Phys. Rev. Lett.* **89**, 233401 (2002).

[3] G. Andresen *et al.*, *Nature* **468**, 673 (2010).

[4] Y. Enomoto *et al.*, *Phys. Rev. Lett.* **105**, 243401 (2010).

[5] G. Gabrielse *et al.*, *Phys. Rev. Lett.* **108**, 113002 (2012).

[6] N. Kuroda *et al.*, *Nature Commun.* **5**, 3089 (2014).

[7] C.H. Storry *et al.*, *Phys. Rev. Lett.* **93**, 263401 (2004).

[8] B.I. Deutch, A.S. Jensen, A. Miranda, G.C. Oades, Proceedings of the First Workshop on Antimatter Physics at Low Energy, Fermilab, Batavia, April 10–12, 1986, p. 371, https://lss.fnal.gov/conf/C860410/p371.pdf

[9] B.I. Deutch *et al.*, *Phys. Scr.* **T22**, 248 (1988).

[10] E.A. Hessels, D.M. Homan, M.J. Cavagnero, *Phys. Rev. A* **57**, 1668 (1998).

[11] M. Charlton, *Phys. Lett. A* **143**, 143 (1990).

[12] M. Charlton, J.W. Humberston, *Positron Physics*, Cambridge University Press, 2000, chapter 6.

[13] G. Drobychev *et al.*, Proposal for the AEgIS experiment at the CERN antiproton decelerator (Antimatter Experiment: Gravity, Interferometry, Spectroscopy), CERN-SPSC-2007-017 (2007).

[14] S. Mariazzi P. Bettotti, R.S. Brusa, *Phys. Rev. Lett.* **104**, 243401 (2010).

[15] S. Aghion *et al.*, *Nucl. Instrum. Methods Phys. Res. B* **407**, 55 (2017).

[16] S. Aghion *et al.*, *Nature Commun.* **5**, 4538 (2014).

[17] S. Aghion *et al.*, *Phys. Rev. A* **94**, 012507 (2016).

[18] S. Aghion *et al.*, *Eur. Phys. J. D* **72**, 76 (2018).

[19] C. Amsler *et al.*, *Nucl. Instrum. Methods Phys. Res. B* **457**, 44 (2019).

[20] F. Castelli, I. Boscolo, S. Cialdi, M.G. Giammarchi, *Phys. Rev. A* **78**, 052512 (2008).

[21] D. Krasnicky, R. Caravita, C. Canali, G. Testera, *Phys. Rev. A* **94**, 022714 (2016).

[22] D. Krasnicky G. Testera, N. Zurlo, *J. Phys. B* **52**, 115202 (2019).

[23] N. Zurlo *et al.*, *Hyperfine Interact.* **240**, 18 (2019).

[24] P. Yzombard *et al.*, *JPS Conf. Proc.* **18**, 011026 (2017).

[25] G. Consolati *et al.*, *Acta Phys. Pol. A* **132**, 1443 (2017).

[26] M. Doser *et al.*, *Phil. Trans. R. Soc. A* **376**, 20170274 (2018).

[27] G.F. Knoll, *Radiation Detection and Measurement*, 4th Edition, John Wiley & Sons Inc., 2010.

[28] CAEN Technical Information Manual, Mod. V1720 8 Channel 12bit–250MS/s Digitizer, Revision No. 26 (2014).

[29] CAEN Technical Information Manual, Mod. V792 series & MOD. V792 N series, 32/16 CH QDCs, Revision No. 18 (2010).

[30] S. Agostinelli *et al.*, *Nucl. Instrum. Methods Phys. Res. A* **506**, 250 (2003).

[31] I. Hrivnacova *et al.*, *The Virtual Monte Carlo*, Computing in High Energy and Nuclear Physics, La Jolla, March 24–28, 2003 [arXiv:cs.SE/0306005].

[32] C. Amsler, *Rev. Mod. Phys.* **70**, 1293 (1998).